

# A unique predator in a unique ecosystem: modelling the apex predator within a Late Cretaceous crocodyliform-dominated fauna from Brazil

Felipe C. Montefeltro<sup>1,2</sup>  | Stephan Lautenschlager<sup>2</sup> | Pedro L. Godoy<sup>3</sup>  |  
Gabriel S. Ferreira<sup>4</sup>  | Richard J. Butler<sup>2</sup> 

<sup>1</sup>Laboratório de Paleontologia e Evolução de Ilha Solteira, UNESP, Ilha Solteira, Brazil

<sup>2</sup>School of Geography, Earth and Environmental Sciences, University of Birmingham, Birmingham, UK

<sup>3</sup>Department of Anatomical Sciences, Stony Brook University, Stony Brook, NY, USA

<sup>4</sup>Departamento de Biologia, Faculdade de Filosofia, Ciências e Letras de Ribeirão Preto, Universidade de São Paulo, Ribeirão Preto, Brazil

## Correspondence

Felipe C. Montefeltro, Laboratório de Paleontologia e Evolução de Ilha Solteira, UNESP, Ilha Solteira, Brazil.  
Email: felipeccmontefeltro@gmail.com

## Funding information

Fundação de Amparo à Pesquisa do Estado de São Paulo, Grant/Award Number: FAPESP 2019/10620-2; National Science Foundation, Grant/Award Number: NSF DEB 1754596; Rutherford Fund Strategic Partner Grant

## Abstract

Theropod dinosaurs were relatively scarce in the Late Cretaceous ecosystems of southeast Brazil. Instead, hypercarnivorous crocodyliforms known as baurusuchids were abundant and probably occupied the ecological role of apex predators. Baurusuchids exhibited a series of morphological adaptations hypothesized to be associated with this ecological role, but quantitative biomechanical analyses of their morphology have so far been lacking. Here, we employ a biomechanical modelling approach, applying finite element analysis (FEA) to models of the skull and mandibles of a baurusuchid specimen. This allows us to characterize the craniomandibular apparatus of baurusuchids, as well as to compare the functional morphology of the group with that of other archosaurian carnivores, such as theropods and crocodylians. Our results support the ecological role of baurusuchids as specialized apex predators in the continental Late Cretaceous ecosystems of South America. With a relatively weak bite force (~600 N), the predation strategies of baurusuchids likely relied on other morphological specializations, such as ziphodont dentition and strong cervical musculature. Comparative assessments of the stress distribution and magnitude of scaled models of other predators (the theropod *Allosaurus fragilis* and the living crocodylian *Alligator mississippiensis*) consistently show different responses to loadings under the same functional scenarios, suggesting distinct predatory behaviors for these animals. The unique selective pressures in the arid to semi-arid Late Cretaceous ecosystems of southeast Brazil, which were dominated by crocodyliforms, possibly drove the emergence and evolution of the biomechanical features seen in baurusuchids, which are distinct from those previously reported for other predatory taxa.

## KEYWORDS

Baurusuchidae, finite element analysis, Notosuchia

## 1 | INTRODUCTION

In nearly all known continental Cretaceous ecosystems worldwide, the dominant hypercarnivores and apex predators were theropod dinosaurs (Lloyd *et al.*, 2008; Benson *et al.*, 2013; Zanno and Makovicky,

2013). However, in the Late Cretaceous ecosystems of Brazil, theropods were exceptionally scarce. Instead, the putative dominant apex predators were a group of large, terrestrial crocodyliforms, the baurusuchids (Riff and Kellner, 2011; Godoy *et al.*, 2014). Baurusuchids are phylogenetically included within Notosuchia, a group of highly

diverse crocodyliforms which thrived mainly in Gondwana during the Cretaceous (Pol and Leardi, 2015; Mannion *et al.*, 2015). Exhibiting a wide range of morphological variation, from gracile omnivores to pug-nosed herbivores, notosuchians significantly contributed to the highest peak of morphological disparity experienced by crocodyliforms across their evolutionary history (Wilberg, 2017; Godoy *et al.*, 2019; Melstrom and Irmis, 2019; Godoy, 2020).

Although present in other parts of Gondwana, most baurusuchid species (ca. 80%) are found in the Late Cretaceous rocks of the Bauru Group in southeast Brazil (Carvalho *et al.*, 2005; Montefeltro *et al.*, 2011; Godoy *et al.*, 2014). The Bauru Group palaeoecosystem witnessed an extraordinary abundance of notosuchians, with nearly 30 species described so far. While dinosaurs were also present, their fossil record in this rock sequence is relatively poor (Montefeltro *et al.*, 2011; Godoy *et al.*, 2014). Within this crocodyliform-dominated ecosystem, baurusuchids are the likely apex predators. Baurusuchids exhibited a series of morphological adaptations hypothesized to be associated with their role as terrestrial hypercarnivores, possibly achieved via heterochronic transformations, such as hypertrophied canines, a reduced number of teeth, and dorsoventrally high skulls (Montefeltro *et al.*, 2011; Riff and Kellner, 2011; Godoy *et al.*, 2018; Wilberg *et al.*, 2019). However, quantitative assessments of the palaeobiology of baurusuchids are lacking, and the data supporting their role as apex predators are primarily derived from broad generalizations and the faunal composition of the Bauru palaeoecosystem (Riff and Kellner, 2011; Godoy *et al.*, 2014).

Here, we employ a biomechanical modelling approach in a comparative investigation of the functional morphology of a baurusuchid (*Baurusuchus*), one analogue of a possible ecological competitor (*Allosaurus*), and an extant crocodyliform (*Alligator*). Using finite element analysis (FEA), we characterize the baurusuchid skull biomechanically and quantify functional similarities and differences between baurusuchids, theropod dinosaurs and living crocodylians. We also calculate bite forces, simulate functional scenarios and conduct bending tests to reveal biomechanical properties of the baurusuchid skull. Our results shed light on key biomechanical aspects that may have allowed this group to dominate the unique ecosystems present during the Cretaceous in Brazil.

## 2 | METHODS

### 2.1 | Specimens

The baurusuchid specimen modelled for the present study is a complete skull with lower jaws, referred to as *Baurusuchus pachecoi* (LPRP/USP 0697 Laboratório de Paleontologia USP-RP, Figure 1a) and collected in Jales, Brazil (Adamantina Formation, Bauru Group; Montefeltro, 2019). *Baurusuchus* is a typical baurusuchid, presenting the set of anatomical traits that characterizes Baurusuchidae and therefore being representative of the clade as a whole (Montefeltro *et al.*, 2011; Godoy *et al.*, 2014). The specimen used for this study has a basal skull length of 33.10 cm (see Table 1

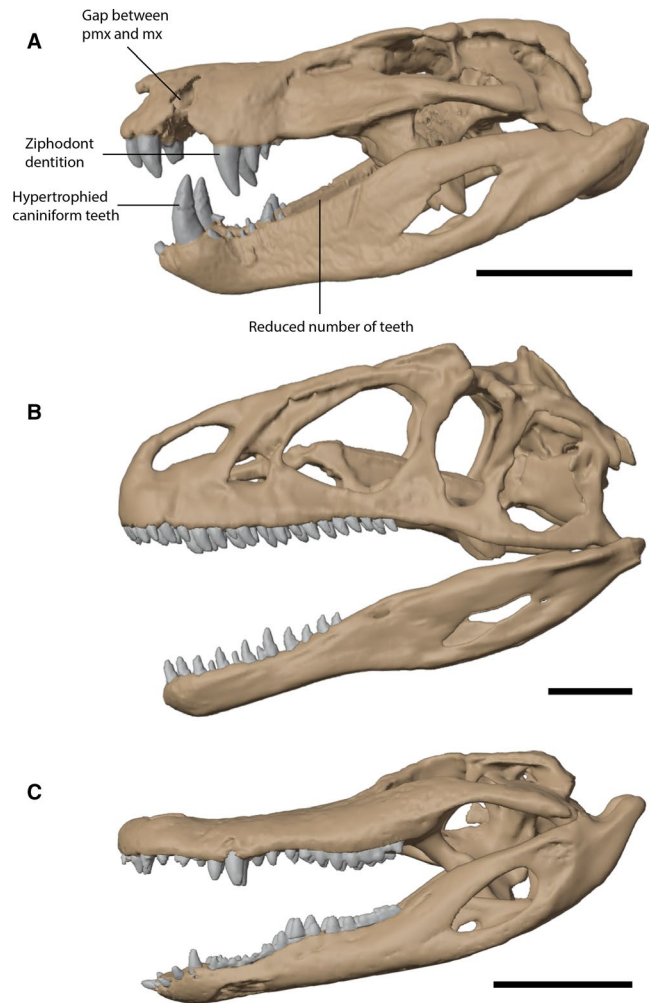


**FIGURE 1** Digitally restored models of skulls used in this study. (a) *Baurusuchus* (LPRP/USP 0697) in lateral view showing typical traits of the members of the clade. (b) *Allosaurus fragilis* (MOR 693) in lateral view. (c) *Alligator mississippiensis* (OUVC 9761) in lateral view. mx: maxilla; pmx: premaxilla

for more cranial measurements) and an estimated total body length of approximately 170 cm, based on the preserved portions of the skeleton (Montefeltro, 2019). Compared with other relatively complete skeletons of adult baurusuchids, such as *Aplestosuchus sordidus* and *Baurusuchus albertoi*, the specimen LPRP/USP 0697 represents a medium-sized baurusuchid (Godoy *et al.*, 2016), with the basal skull length being 70% that of the holotype of *Stratiotosuchus maxhechti* (one of the largest complete skulls known among baurusuchids; Riff and Kellner, 2011; Godoy *et al.*, 2016).

For comparison, we modelled a specimen of the theropod dinosaur *Allosaurus fragilis* (MOR 693, Museum of the Rockies, Bozeman, Figure 1b) and one specimen of *Alligator mississippiensis* (OUVC 9761, Ohio University Vertebrate Collections, Figure 1c) (see Rayfield *et al.*, 2001 and Witmer and Ridgely, 2008 for scanning details). *Allosaurus fragilis* was chosen based on its medium size compared with other theropods, which is equivalent to the putative size of the theropods from the Adamantina Formation, for which no complete craniomandibular material is currently

**TABLE 1** Selected measurements (in cm) for the skull LPRP/USP 0697

LPRP/USP 0697	
Basal skull length (from tip of snout to occipital condyle along midline)	33.10
Length of skull (from posterior end of skull table to tip of snout, on midline)	30.20
Length of snout (from anterior end of orbit to tip of snout)	18.27
Greatest transverse width of skull (across quadratojugals)	17.99
Least transverse interorbital distance	4.65
Transverse width of skull at level of anterior ends of orbits	7.13
Transverse width of skull at level of postorbital bars	9.59
Transverse width of skull table anteriorly	10.16
Transverse width of skull table posteriorly	15.23

known. Furthermore, *Allosaurus* has been proposed to be functionally similar to abelisaurids, the most commonly found theropods in the Bauru Group (Sakamoto, 2010). The choice of *Alligator mississippiensis* (as a living representative of the crocodyliform lineage) was made because this is a model organism for herpetological and functional studies (Guillette *et al.*, 2007; Farmer and Sanders, 2010; Reed *et al.*, 2011). For the subsequent FEA, existing 3D models of *Allo. fragilis* and *A. mississippiensis* from previous studies were used (Rayfield *et al.*, 2001; Witmer and Ridgely, 2008; Lautenschlager, 2015). The *B. pachecoi* skull was scanned in a Toshiba Aquilion Prime machine, at the Hospital das Clínicas de Ribeirão Preto, Brazil. The scan resulted in 1917 projections, generating 1,187 slices (thickness of .5 cm), voltage of 120 kV, and current of 150  $\mu$ A. The segmentation of bones was performed with AMIRA 5.3 (Thermo Fisher Scientific).

## 2.2 | FEA

The 3D models of all specimens, including skulls and mandibles, were imported into Hypermesh 11 (Altair Engineering) for the generation of solid tetrahedral meshes (consisting of approximately 1,000,000 elements per model). For the *Alligator* and the baurusuchid models, material properties for bone and teeth were assigned based on values for *A. mississippiensis* (bone:  $E = 15.0$  GPa,  $\nu = .29$ , teeth:  $E = 60.4$  GPa,  $\nu = .31$ ; Porro *et al.*, 2011; Sellers *et al.*, 2017), whereas for the *Allosaurus* model, values were derived from studies on theropods (bone:  $E = 20.0$  GPa,  $\nu = .38$ , teeth:  $E = 60.4$  GPa,  $\nu = .31$ ; Rayfield *et al.*, 2001, Rayfield, 2011). To exclude the possibility of different results due to distinct material properties, we also conducted an FEA on the *Allosaurus* model using the same bone and teeth properties assigned to the crocodyliform models. All material properties in the models were assigned in Hypermesh and treated as isotropic and homogeneous.

Intrinsic scenarios for the baurusuchid *Allo. fragilis* and *A. mississippiensis* were simulated for the skull and lower jaw models, using a simplified jaw adductor muscle-driven biting. The adductor muscle forces of the baurusuchid were estimated using the attachment area for each muscle (Figure 2), based on previous works on extant and extinct crocodyliforms (Holliday and Witmer, 2009;

Holliday *et al.*, 2013). The adductor chamber reconstruction of the dinosaur and crocodylian was based on previously published data for the muscle arrangements for both taxa (Rayfield *et al.*, 2001; Rayfield, 2011; Porro *et al.*, 2011; Sellers *et al.*, 2017). The attachment areas measured for the three taxa were used as a proxy for physiological cross-sectional area, which was then multiplied by an isometric muscle stress value of  $25.0 \text{ N cm}^{-2}$  (Porro *et al.*, 2011). Table 2 shows the total muscle force inferred for each muscle. Although this isometric muscle stress is on the lower margin of the range of values reported for vertebrate muscles (e.g. 32 and  $35 \text{ N/cm}^2$ ) it was selected here due to the relatively close phylogenetic position of baurusuchids to modern crocodylians. However, the calculated bite force would be only slightly (10%–15%) higher using different values for isometric muscle stress. Three intrinsic scenarios were analysed to estimate the muscle-driven biting force in the baurusuchid:

- a bilateral bite at the second maxillary and the fourth dentary tooth,
- a unilateral bite at the second maxillary and the fourth dentary tooth
- a unilateral bite at the third premaxillary tooth.

One intrinsic scenario was analysed for both *Allo. fragilis* and *A. mississippiensis*: the maxillary and dentary unilateral bite scenarios. For each intrinsic scenario in all taxa, constraints were placed on nodes at the craniomandibular articular surfaces. Each node was constrained in all directions (x, y, z). For the skulls, three nodes were constrained on the occipital condyle and two nodes on each quadrate articular surface. For the lower jaws, three (baurusuchid) or four (*Allosaurus* and *Alligator*) nodes on each glenoid were constrained. To estimate the biting force of the baurusuchid, nodes were constrained at the tip of the teeth to measure the reaction force caused by the modelled adductor muscles; the same approach was used for the other two taxa. In unilateral scenarios, the tip of one tooth was constrained, whereas in bilateral scenarios, the tips of the teeth on both sides were constrained. The constrained teeth were PM3, M2 and D4 for the baurusuchid, M3 and D5 for *Allo. fragilis*, and M4 and D4 for *A. mississippiensis*. The intrinsic scenarios were all based on the same jaw adductor reconstructions for each taxon and aimed

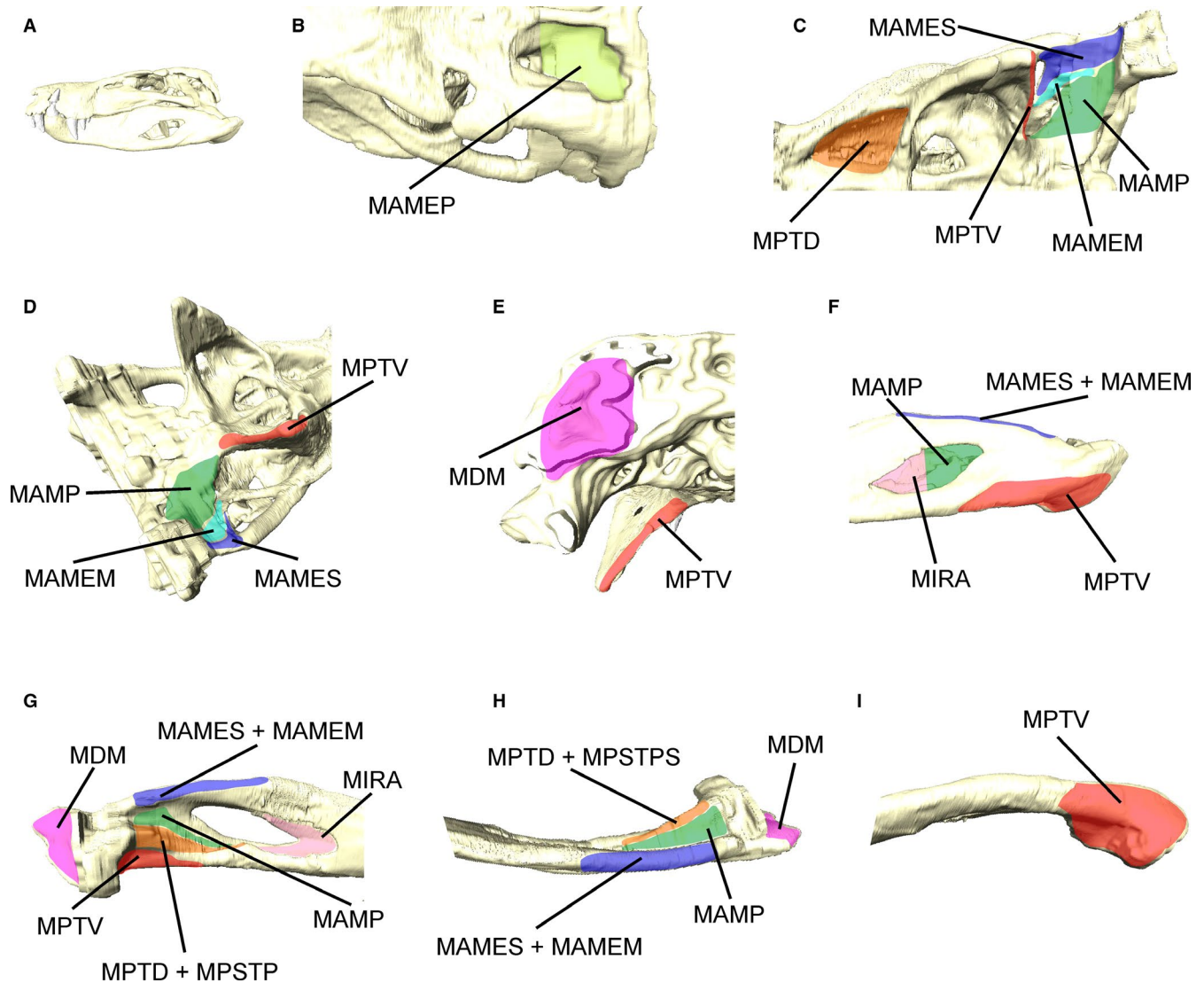


**FIGURE 2** Muscle attachment areas plotted on the 3D model of skull the baurusuchid LPRP/USP 0697. (a) Skull and lower jaws in lateral view. (b) Dorsal view of the left posterior of the skull. (c) Ventral view of the left posterior of the skull. (d) Posterolateral view of the skull. (e) Occipital view of the left portion of the skull. (f) Lateral view of the posterior portion of the left mandibular ramus. (g) Medial view of the posterior portion of the left mandibular ramus. (h) Occlusal view of the posterior portion of the left mandibular ramus. (i) Ventral view of the posterior portion of the left mandibular ramus. MAMEM: *m. adductor mandibulae externus medialis*; MAMEP: *m. adductor mandibulae externus profundus*; MAMES: *m. adductor mandibulae externus superficialis*; MAMP: *m. adductor mandibulae posterior*; MDM: *m. depressor mandibulae*; MIRA: *m. intramandibularis*; MPSTPS: *m. pseudotemporalis profundus*; MPTD: *m. pterygoideus dorsalis*; MPTV: *m. pterygoideus ventralis*

to emulate possible behaviors of baurusuchids, theropod dinosaurs and crocodylians.

To investigate the craniomandibular biomechanical properties in alternative load assignments, five bending scenarios were also tested for the baurusuchid skull and mandible models: unilateral bending, bilateral bending, pull-back, head-shake and head-twist. The bending test scenarios were proposed as an additional investigation of the skull properties in situations that approach behaviors during different types of strikes, including biting (unilateral bending and bilateral bending) and supplementary head movements allowed by postcranial musculature (pull-back, head-shake and head-twist). The loading applied for each scenario was based on the approximation of the greatest bite force obtained from the intrinsic scenario (600 N; see results below). All loadings in the unilateral bending scenario were applied to

one node, perpendicular to the occlusal planes on one of the following teeth: D1, D4, D9, PM2, PM3, M2 and M4. Bilateral bending scenarios were tested with the same conditions as the unilateral ones but with two vectors of 300 N applied symmetrically to each canine at the M4 and the D4. The head-shake scenario was tested with two vectors of 300 N pointing in the same direction, one on one node on the labial surface of left M2/D4 and the other on one node on the lingual surface of right M2/D4. For the pull-back, the load force of 600 N was applied to one node at crown midheight over the distal carina of the caniniform teeth (D4, PM3 and M2). For the head twist, the loadings were applied to two opposite vectors of 300 N in each model. One loading vector was applied to one node at the tip of the maxillary (M2) or dentary (D4) caniniform tooth and another loading vector on the opposite side on the dorsal surface of the maxilla or ventral surface of the dentary.

Four bending scenarios were also tested in the skull and lower jaws of *Allo. fragilis* and *A. mississippiensis* for comparison. Unilateral and bilateral bending simulated the comparable positions of that tested in the baurusuchid. Unilateral bending was tested in PM2, M3, M16, D1, D4 and D13 for *Allo. fragilis*, and PM2, M4, M15, D2, D4 and D15 for *A. mississippiensis*. Bilateral bending was also tested in M3 and D5 pairs for the theropod and in M4 and D4 pairs for

the crocodylian. For meaningful comparisons of form and function independent of size (Dumont *et al.*, 2009), all models used in the bending tests were scaled to the total surface of the baurusuchid specimen. For the bending scenarios, constraints were placed on the same nodes as in the intrinsic scenarios. The performances for the FEA models were assessed via contour plots of von Mises stress distribution and mean von Mises stress and displacement values per element. To avoid the influence of individual stress singularities, such as at the constrained or loaded nodes, we used an averaging threshold of 99%.

**TABLE 2** Total force inferred from cranial and lower jaw attachments for each muscle modeled

Muscle	Total muscle force (N)
<i>m. adductor mandibulae externus medialis</i>	132.65
<i>m. adductor mandibulae externus profundus</i>	227.625
<i>m. adductor mandibulae externus superficialis</i>	157.875
<i>m. adductor mandibulae posterior</i>	249.475
<i>m. depressor mandibulae</i>	245.925
<i>m. intramandibularis</i>	87.775
<i>m. pseudotemporalis profundus</i>	61.25
<i>m. pterygoideus dorsalis</i>	235.94
<i>m. pterygoideus ventralis</i>	198.4

**3 | RESULTS**

During the bilateral bite scenario, the bite force estimate for the baurusuchid specimen was 252 N for the skull and 578 N for the lower jaw. For the premaxillary unilateral bite scenario, bite force was estimated as 199 N, whereas for both maxillary and lower jaw unilateral bite scenarios, it was 450 N. The distribution and magnitude of the von Mises stress showed little difference in the intrinsic scenarios for the skull and lower jaw of the baurusuchid (Figure 3). Most of the elements in the skull remained relatively stress-free in the three

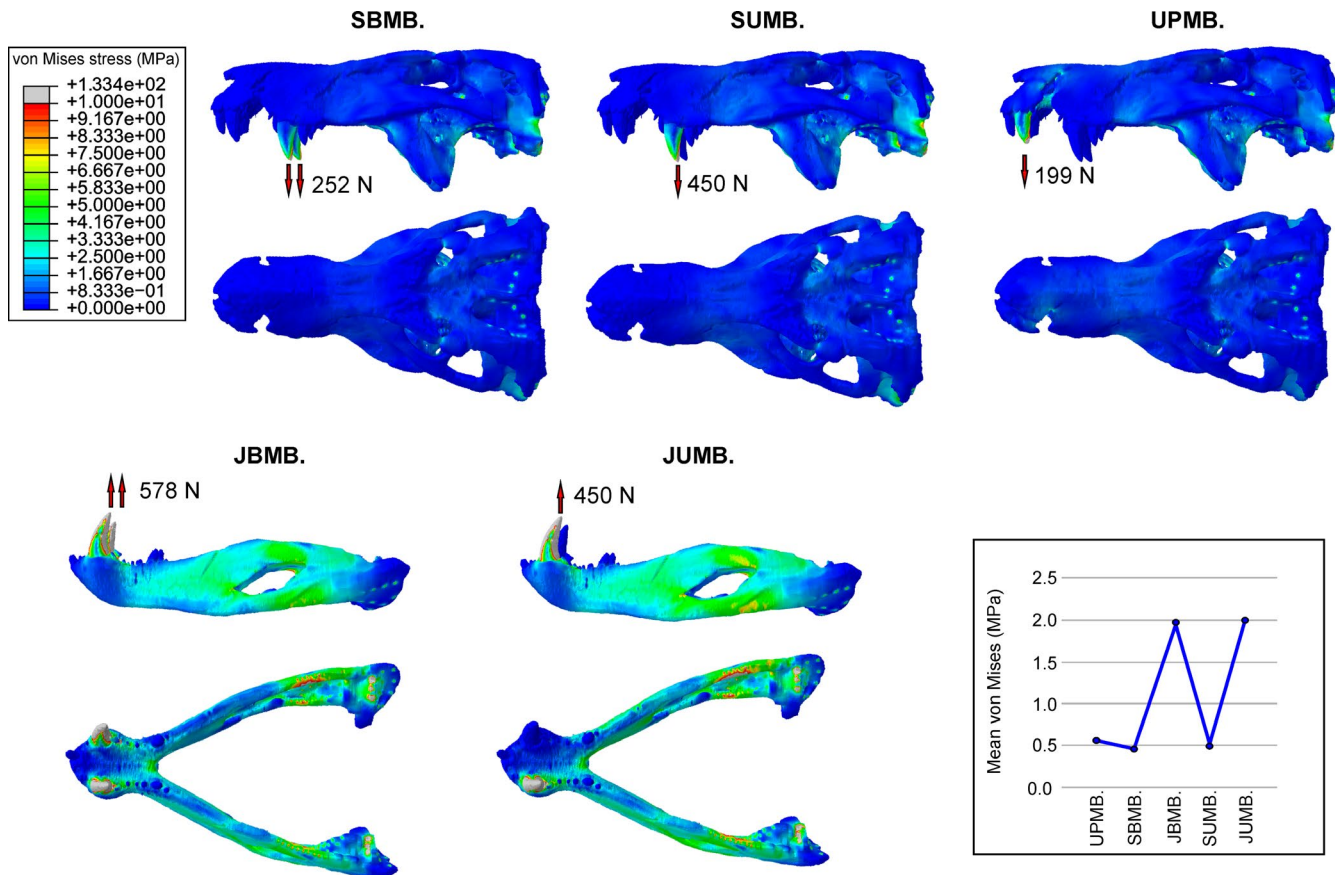


**FIGURE 3** Von Mises stress contour plots from finite elements analysis (FEA) of the baurusuchid specimen (LPRP/USP 0697) for the intrinsic scenarios. Arrows indicate the location of muscle-driven bite forces on models during each scenario, with respective estimated bite force values. Mean von Mises values per scenario are displayed on the bottom right. JBMB.: jaw bilateral muscle-driven bite; JUMB.: jaw unilateral muscle-driven bite; SBMB.: skull bilateral muscle-driven bite; SUMB.: skull unilateral muscle-driven bite; UPMB.: unilateral premaxillary muscle-driven bite

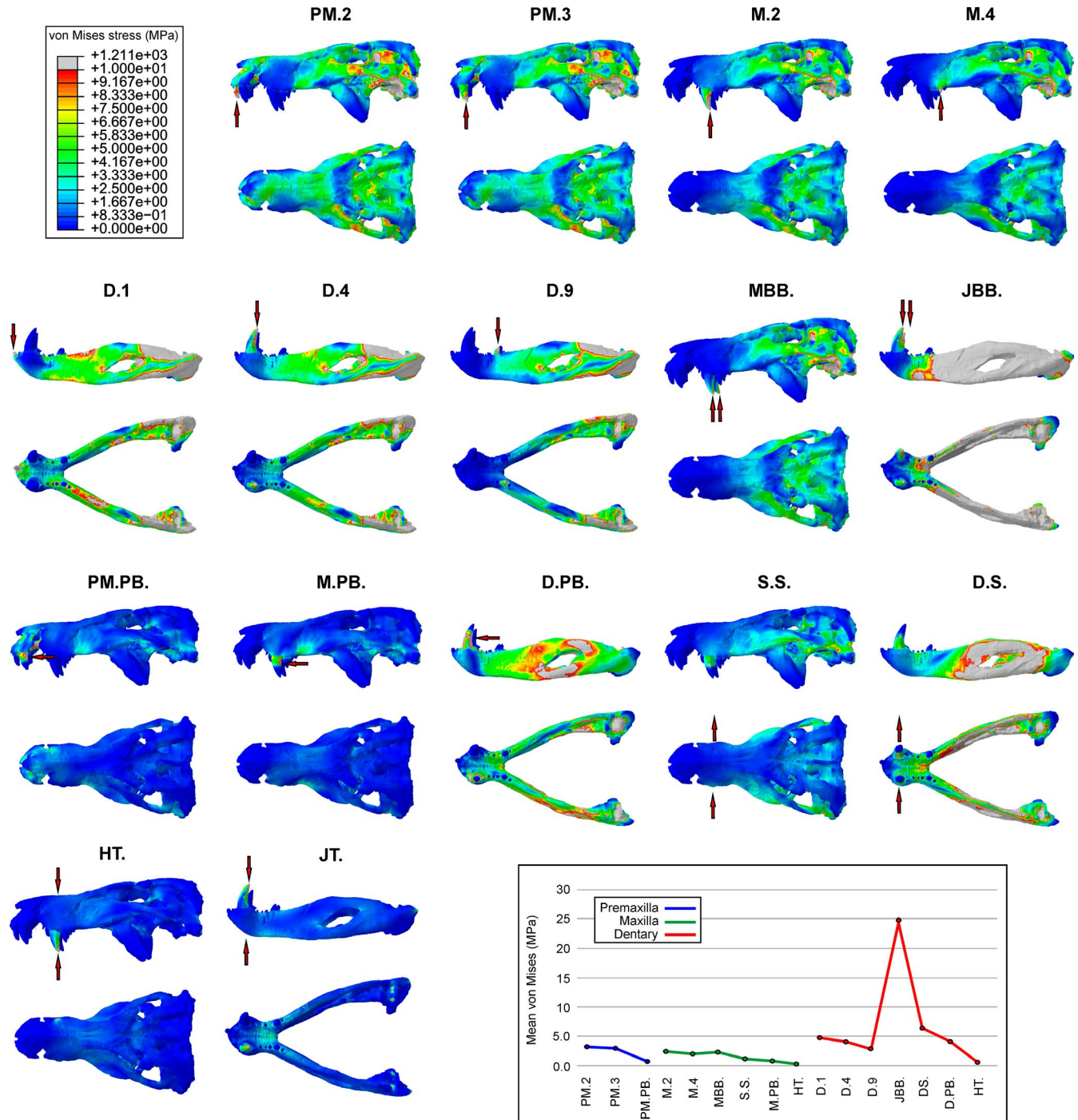


**FIGURE 4** Von Mises stress contour plots from FEA of the baurusuchid specimen LPRP/USP 0697, comparing the stress distribution of skull and mandible models under distinct functional bending scenarios. Arrows indicate the location on the models of the loading vectors for each scenario. Mean von Mises values per scenario are displayed on the bottom right. D.1.: jaw anterior unilateral bending; D.4.: jaw canine unilateral bending; D.PB.: dentary canine pull-back; D.S.: canine dentary shake; HT.: head-twist (skull); JBB.: jaw canine bilateral bending; JT.: head-twist (jaw); M.2.: maxilla canine unilateral bending; M.4.: maxilla posterior unilateral bending; MBB.: maxilla canine bilateral bending; M.PB.: maxilla canine pull-back; PM.2.: premaxilla anterior unilateral bending; PM.3.: premaxilla canine unilateral bending; PM.PB.: premaxilla canine pull-back; S.S.: canine skull shake

intrinsic scenarios simulated (mean von Mises stress of .46 MPa during the bilateral maxillary biting, .50 MPa during the unilateral maxillary biting and .52 MPa during the premaxillary unilateral biting). The quadrate body, the body of the ectopterygoid and the posterior margin of the pterygoid are the main regions in which stresses are

present during those simulated scenarios (Figure 3). In the intrinsic scenario for the premaxillary canine bite, there is also increased stress at the anterior margin of the notch between the premaxilla and maxilla, which also extends medially, surrounding the notch at the secondary bony palate. As expected, the lower jaws experienced

more von Mises stress compared with the skull model (mean von Mises stress of 1.93 MPa in the bilateral biting and 2.01 MPa in the unilateral biting). In both scenarios, the symphyseal region surrounding the canine teeth and the retroarticular process remained relatively stress-free; the greatest von Mises stress was observed on the dorsal surface of the surangular and ventral surface of the angular.

Considerable differences were found between the von Mises stress magnitudes of the skull and lower jaws of the baurusuchid in the different bending scenarios tested (e.g. mean values of .4 MPa in the skull head twist and 24.7 MPa in the bilateral biting of the lower jaws). Although variable in magnitude, a general pattern is discernible in the stress distribution in the skull and lower jaws of the baurusuchid (Figure 4). The greatest von Mises stresses in the skull models are mostly present in the posterior and median portions of the skull, with stress hotspots located on the ventral and lateral regions of the quadrate body, ventral region of the infratemporal bar and preorbital region (anterior jugal, posterior maxillae, lacrimals, nasal, prefrontals and anterior frontal). In addition, the areas of maximum von Mises stress in the premaxillae and maxillae are isolated from each other. This means that when loading is applied to the premaxillary teeth, the maxillae remain relatively stress-free, whereas the dorsal rostrum (premaxilla and nasals) is more stressed. When loading is applied to the maxillary teeth, the premaxillae remain unstressed, and stress is concentrated on the posterior portion of the skull (Figure 4).

The lower jaws also experienced more von Mises stress than the skull model during the bending tests, and the stress hotspots were

more homogeneously distributed, located on the dorsal surface of the surangular, angular and retroarticular process. Two exceptions are the jaw pull-back scenario, in which the stress hotspots are located around the mandibular fenestra, and the bilateral bending scenario, in which most of the lower jaw is highly stressed and only the symphyseal region remains less stressed.

The areas around the maxillary and dentary canines remain relatively stress-free, even during scenarios in which the loadings were applied to the canines (both in the intrinsic scenarios and in the bending tests). This is particularly evident for the dentary canine, for which the surrounding bone remains unstressed in all scenarios, including the least optimal scenario of bilateral bending (Figure 4).

In general, the patterns of von Mises stress distribution obtained for *Allosaurus* and *Alligator* (Figures 5 and 6) were consistent with previous studies (Rayfield *et al.*, 2001; Porro *et al.*, 2011). Even considering that the bone properties assigned to the *Allosaurus* are slightly different from the other models, this did not substantially change the results obtained from this taxon. Considering the intrinsic scenarios, the measured mean von Mises stress is similar during maxillary unilateral biting (mean von Mises stress of .72 MPa for *Allosaurus* and .62 MPa for *Alligator*). The pattern of stress distribution observed in the models of the *Alligator* are much closer to that observed in the baurusuchid than the *Allosaurus*, perhaps related to the phylogenetic proximity reflected in the cranial architecture of both crocodyliforms.

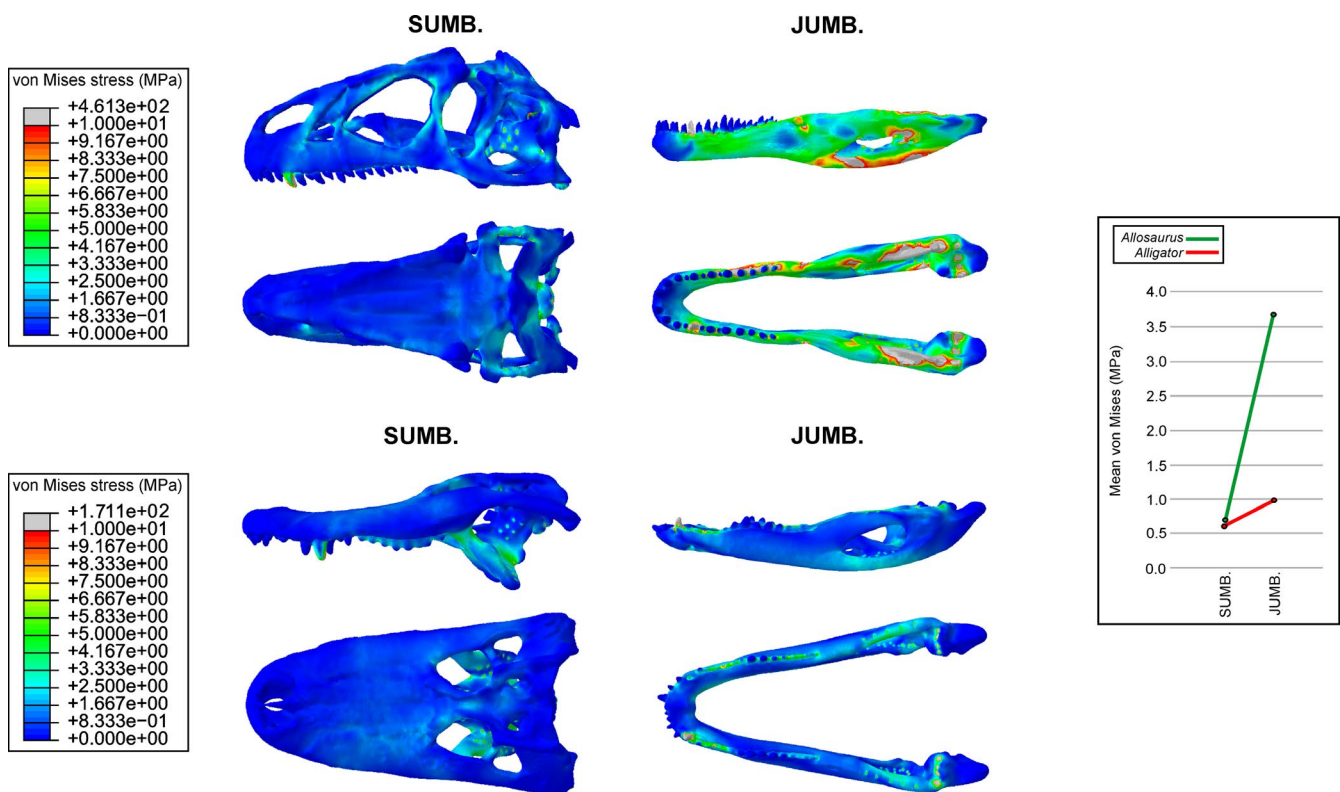


**FIGURE 5** Von Mises stress contour plots from FEA of *Allosaurus fragilis* and *Alligator mississippiensis* for the intrinsic scenarios. Mean von Mises values per scenario for each taxon are displayed on the right. JUMB.: jaw unilateral muscle-driven bite; SUMB.: skull unilateral muscle-driven bite

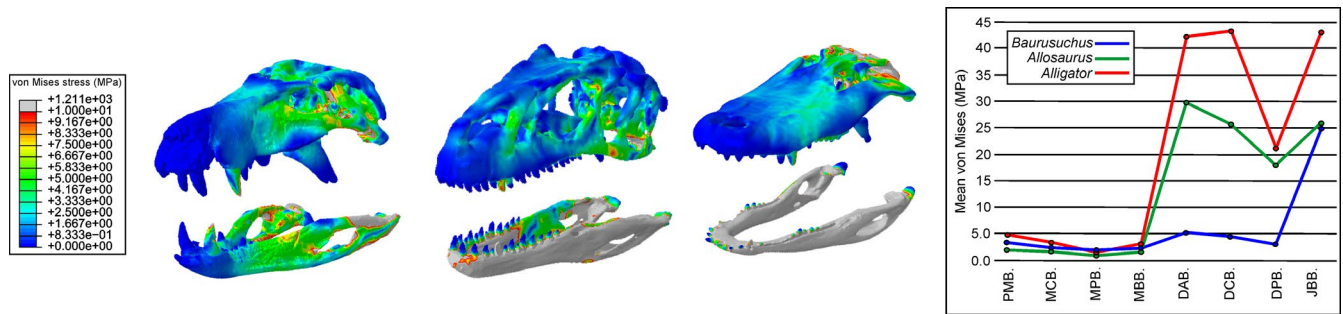


**FIGURE 6** Comparison of von Mises stress distribution for scaled models of different archosaurian carnivores: baurusuchid, *Allosaurus fragilis* and *Alligator mississippiensis*. Stress contour plots displayed for the anterior bending scenario. On the right, comparative mean von Mises values per scenario for each taxon. DAB.: jaw anterior bending; DCB.: jaw canine unilateral bending; DPB.: jaw canine unilateral bending; JBB.: jaw canine bilateral bending; MBB.: maxilla canine bilateral bending; MCB.: maxilla canine unilateral bending, MPB: maxilla posterior unilateral bending; PMB.: unilateral premaxillary bending

Greater differences were found in the two taxa in the lower jaw models during the intrinsic scenarios (mean von Mises stress of 3.7 MPa for *Allosaurus* and .99 MPa for *Alligator*). The discrepancies observed in the bending scenarios are also the most evident in the lower jaws, which for the baurusuchid remains consistently less stressed than either the theropod or the crocodylian during the bending tests. When compared with the baurusuchid, only slightly lower mean von Mises stress values for the skull were obtained in the theropod models, but much higher values for the lower jaws (Figure 6). In the alligator model, in contrast, higher mean von Mises stress values were found in most scenarios than in either the baurusuchid or *Allosaurus*, even though differences in stress values are less distinguishable between skull models of the analysed taxa (Figure 6). The only scenario that does not follow this pattern is the unilateral bending at the back of the upper tooth row, in which the mean von Mises stress value is similar for the baurusuchid and *Alligator*, although both have higher stresses than the theropod. The most divergent results are related to the mandibular anterior bending scenario, in which the mean stress value in *Alligator* was more than nine times higher than in the baurusuchid, and almost twice the mean von Mises stress recorded for the theropod.

## 4 | DISCUSSION

The unexpectedly weak bite force estimated for the baurusuchid is much lower than that measured for extant crocodylians of comparable size. For example, *Alligator sinensis* has a similar total body length (150–200 cm) and can have a bite of up to 963 N (measured at the caniniform tooth), whereas *Paleosuchus* is the only living species with comparable bite force values to the baurusuchid modeled (Erickson *et al.*, 2012). The bite force estimated for the baurusuchid is also only a fraction of the bite forces inferred for adult theropods, which could potentially exceed 50,000 N (Gignac and Erickson, 2017). Furthermore, to estimate the bite force of extinct crocodylians, previous studies have applied equations based on regression data from extant crocodylians (e.g. Aureliano *et al.*, 2015). Although this type of equation is likely to provide a relatively correct estimate of

the bite force for fossil crocodylians phylogenetically close to the Crocodylia clade and sharing the basic cranial architecture, the equation does not take into consideration the very different cranial architectures present in more distantly related taxa such as baurusuchids. As a result, the equation may not be accurate for anatomically divergent taxa and will overestimate or underestimate the bite forces of those taxa. We applied the equations presented by Aureliano *et al.* (2015), which use data from living species (Verdade, 2000; Erickson *et al.*, 2012), to the craniomandibular measurements of the specimen studied here (LPRP/USP 0697) and obtained a much higher bite force estimation (of nearly 4,000 N). This apparent overestimation demonstrates that the differences between the cranial structures of living and extinct crocodylians may have important functional implications, such as the disproportionately positive bite force increase previously inferred for baurusuchids (Gignac and O'Brien, 2016).

In this context, it is noteworthy that the bite force estimates from FEA vary when using the skull or the mandible to obtain reaction forces. This is not surprising, as the geometry and architecture of the skull is more complex and subject to further constraints than in the mandible. Validation tests have shown, however, that realistic bite forces can be estimated from mandible models (Porro *et al.*, 2011). Consequently, we consider the higher bite force values obtained from the mandible to be the more likely for the baurusuchid.

The comparatively weak bite force in baurusuchids suggests that their role as apex predators may have involved hunting strategies different from those of most carnivorous theropods and living crocodylians, which mostly rely on muscle-driven biting forces for killing (Rayfield, 2004, 2005, 2011; D'Amore *et al.*, 2011; Erickson *et al.*, 2012). As a consequence, the killing potential of baurusuchids could have been enhanced by structural and behavioral traits, as in other weak-bite apex predators such as troodontid and allosaurid theropods, varanid lizards and felines, all of which harness the postcranial musculature to supplement bite force (Rayfield *et al.*, 2001; D'Amore *et al.*, 2011; Figueirido *et al.*, 2018; Torices *et al.*, 2018).

Alternatively, the apex predator role of baurusuchids could have been a historical misinterpretation and the group might be better interpreted as preying on smaller and/or softer animals. However, a series of craniomandibular and postcranial adaptations

of baurusuchids indicate otherwise. For example, the presence of extensive overengineered regions around the canines in both the skull and lower jaws (e.g. regions that remain relatively stress-free in all tests) show that the baurusuchid craniomandibular architecture could safely perform in much higher stress conditions than imposed by muscle-driven biting forces. This is true even for our bending tests, which most likely overestimate the stress experienced by the skull of the baurusuchid. The presence of overengineered regions in *Allosaurus* has been proposed as evidence that this taxon also used mechanisms to enhance killing potential in its regular feeding strategy (Rayfield *et al.*, 2001).

Additionally, the tested pull-back, head-shake and head-twist scenarios were designed to understand how the baurusuchid craniomandibular architecture would perform during similar head movements employed by other weak- and strong-bite apex predators (Rayfield *et al.*, 2001; D'Amore *et al.*, 2011; Torices *et al.*, 2018). For baurusuchids, these movements would be possible given the robust cervical vertebrae, high neural spines and well-developed cervical ribs (particularly the first two), which provided large attachment areas for the muscles responsible for head lift, head twist and side-to-side movements (Cleuren and De Vree, 2000; Godoy *et al.*, 2018). These tests show that the baurusuchid skull and mandible worked optimally in scenarios simulating non-orthal loads, suggesting that baurusuchids were well-suited for head movements during predation, possibly even more so than living crocodylians. This can be explained by the combination of three skull features that minimize skull stress during bites and torsion: the oreinostral morphology, the absence of the antorbital fenestra and the extensively ossified secondary palate. This combination of features is particularly efficient for stress reduction during unilateral biting (Rayfield and Milner, 2008).

Our tests also revealed that the well-developed gap between premaxillae and maxillae is a unique specialization in the skull architecture of baurusuchids, very likely related to predatory habits. This gap redirects the stress from the premaxillae to the dorsal surface of the fused nasals during biting, preventing stress from travelling from the occlusal region of one bone to the other and implying a functional decoupling between premaxillae and maxillae during bites. This gap at the premaxillae-maxillae suture is absent in *Allosaurus* and *Alligator* and, in those taxa, the stress travels directly from the premaxilla to the maxilla, especially during the unilateral premaxillary bending scenarios. A similar stress redirection is observed in tyrannosaurids, in which the robust and also fused nasals work as the main route for stress distribution, bypassing the less robust maxilla-lacrimal contact (Rayfield, 2005). We suggest that the gap observed in baurusuchids, in combination with the robust and fused nasals, worked similarly to that of tyrannosaurids, although the general cranial architecture presented by the baurusuchid is closer to the *Alligator*. The gap could also allow repeated punctures to be inflicted from biting at different positions of the tooth row, but concomitantly working as a built-in safety factor, minimizing the risk of the skull yielding (Rayfield *et al.*, 2001). Finally, the presence of ziphodont dentition in baurusuchids is also in line with the role of apex predator (Riff and Kellner, 2011; Godoy *et al.*, 2014). Knife-like teeth with well-developed serrated

cutting edges are a dental adaptation for optimal defleshing of vertebrate carcasses (D'Amore, 2009) and are present in a series of unrelated apex predators, including theropod dinosaurs and large monitor lizards (D'Amore *et al.*, 2011; Brink and Reisz, 2014; Torices *et al.*, 2018).

The discrepancy in the von Mises stress magnitude and distribution seen between the mandibles of the three taxa during the intrinsic scenarios and during the bending tests suggests that this structure is also pivotal in understanding the palaeoecology of baurusuchids. The von Mises stress distribution shows that *Allosaurus* and *Alligator* have, in general, higher and more homogeneously distributed von Mises stress in the mandible, whereas in the baurusuchid the stress is concentrated at the post-symphyseal region. This indicates that the robust symphysis in baurusuchids is important for stabilizing the lower jaws.

The best example of the divergent responses among lower jaws is seen in the bilateral bending scenario, for which the mean von Mises stress value for the baurusuchid was approximately five times greater than in any other scenario. Additionally, this is the only scenario in which the von Mises stress approaches the higher values presented by *Allosaurus* and *Alligator* (Figure 6). The baurusuchid response is also different from *Allosaurus* and *Alligator* in the sense that the mean von Mises stress values in the bilateral bending scenarios are distinct from the unilateral scenarios, whereas the other two taxa show similar values in both scenarios. Based on our FEA results, we propose that the bilateral biting is the least likely killing strategy for baurusuchids, and the clamp-and-hold employed by living crocodylians and large mammal predators such as the lion (*Panthera leo*; Figeirido *et al.*, 2018) does not fit the mechanical properties of the baurusuchid skull.

Our results also indicate that baurusuchids were well adapted for handling struggling prey, which was possibly subdued by inflicting a series of bites using premaxillary, maxillary and, particularly, the dentary canines, which combined with ziphodonty would repeatedly pierce the skin of the prey. The puncture phase would be followed by head movements that would worsen the wounds caused by the punctures, ultimately leading to the death of the prey.

Our results successfully characterize the exceptional suite of biomechanical properties displayed by baurusuchids, which combine novel adaptations as well as features similar to theropods and others seen in living crocodylians. Such a combination has not been reported previously for any predatory taxon, raising questions on the specific evolutionary settings that allowed these features to emerge. Selective pressures from extrinsic environmental factors seem to exert an important influence during amniote functional and biomechanical evolution (Sakamoto *et al.*, 2019). In the case of baurusuchids, the unique Late Cretaceous palaeoecosystems of southeast Brazil exhibited a combination of playa-lake systems and transitory rivers which possibly permitted life to flourish in semi-arid to arid conditions (Carvalho *et al.*, 2010; Marsola *et al.*, 2016). These landmasses witnessed an extraordinary diversity of crocodyliforms (especially notosuchians; Mannion *et al.*, 2015), as well as other tetrapods (Godoy *et al.*, 2014). This resulted in a diverse array

of potential prey for baurusuchids among terrestrial tetrapods, including crocodyliforms and sauropods, indicating that prey selection could have played an important role in the evolution of the baurusuchid craniomandibular apparatus.

## ACKNOWLEDGEMENTS

This work was supported in part by a Rutherford Fund Strategic Partner Grant to the University of Birmingham, which funded the travel of F.C.M. to Birmingham. This research was supported by a National Science Foundation grant (NSF DEB 1754596) to P.L.G. and Fundação de Amparo à Pesquisa do Estado de São Paulo (FAPESP 2019/10620-2) to G.S.F. We thank two reviewers for their comments, which improved the final version of this manuscript. We would like to thank M.C. Langer (USP) for the access to the specimen LPRP/USP 0697, and F.J. Oliveira and M.K. Santos (Hospital das Clínicas de Ribeirão Preto) for the CT scanning of this fossil.

## AUTHOR CONTRIBUTIONS

F.C.M., S.L. and R.J.B. conceived and designed the experiments. F.C.M., S.L. and P.L.G. wrote the paper. All authors analyzed the data, and read and commented on the final version of the article and approved it.

## ORCID

Felipe C. Montefeltro  <https://orcid.org/0000-0001-6519-8546>

Pedro L. Godoy  <https://orcid.org/0000-0003-4519-5094>

Gabriel S. Ferreira  <https://orcid.org/0000-0003-1554-8346>

Richard J. Butler  <https://orcid.org/0000-0003-2136-7541>

## REFERENCES

- Aureliano, T., Ghilardi, A.M., Guilherme, E., Souza-Filho, J.P., Cavalcanti, M. and Riff, D. (2015) Morphometry, bite-force, and paleobiology of the Late Miocene Caiman *Purussaurus brasiliensis*. *PLoS ONE*, 10, e0117944.
- Benson, R.B.J., Mannion, P.D., Butler, R.J., Upchurch, P., Goswami, A. and Evans, S.E. (2013) Cretaceous tetrapod fossil record sampling and faunal turnover: implications for biogeography and the rise of modern clades. *Palaeogeography, Palaeoclimatology, Palaeoecology*, 372, 88–107.
- Brink, K.S. and Reisz, R.R. (2014) Hidden dental diversity in the oldest terrestrial apex predator *Dimetrodon*. *Nature Communications*, 5, 3269.
- Carvalho, I.S., Campos, A.C.A. and Nobre, P.H. (2005) *Baurusuchus salgadoensis*, a new Crocodylomorpha from the Bauru Basin (Cretaceous), Brazil. *Gondwana Research*, 8, 11–30.
- Carvalho, I.S., Gasparini, Z.B., Salgado, L., Vasconcellos, F.M. and Marinho, T.S. (2010) Climate's role in the distribution of the Cretaceous terrestrial Crocodyliformes throughout Gondwana. *Palaeogeography, Palaeoclimatology, Palaeoecology*, 297, 252–262.
- Cleuren, J. and De Vree, F. (2000) Feeding in crocodylians. In: Schwenk, K. (Ed.) *Feeding: Form, Function and Evolution in Tetrapod Vertebrates*. San Diego: Academic Press, pp. 337–358.
- D'Amore, D.C. (2009) A functional explanation for denticulation in theropod dinosaur teeth. *Anatomical Record*, 292, 1297–1314.
- D'Amore, D.C., Moreno, K., McHenry, C.R. and Wroe, S. (2011) The effects of biting and pulling on the forces generated during feeding in the Komodo dragon (*Varanus komodoensis*). *PLoS ONE*, 6, e26226.
- Dumont, E., Grosse, I. and Slater, G. (2009) Requirements for comparing the performance of finite element models of biological structures. *Journal of Theoretical Biology*, 256, 96–103.
- Erickson, G., Gignac, P., Stepan, S., Lappin, A.K., Vliet, K.A., Brueggem, J.D., et al. (2012) Insights into the ecology and evolutionary success of crocodylians revealed through bite-force and tooth-pressure experimentation. *PLoS ONE*, 7, e31781.
- Farmer, C.G. and Sanders, K. (2010) Unidirectional airflow in the lungs of alligators. *Science*, 327, 338–340.
- Figueirido, B., Lautenschlager, S., Pérez-Ramos, A. and Valkenburgh, B. (2018) Distinct predatory behaviors in scimitar- and dirk-toothed sabertooth cats. *Current Biology*, 28, 3260–3266.
- Gignac, P. and Erickson, G. (2017) The Biomechanics behind Extreme Osteophagy in *Tyrannosaurus rex*. *Scientific Reports*, 7, 2012.
- Gignac, P. and O'Brien, H. (2016) Suchian feeding success at the interface of ontogeny and macroevolution. *Integrative and Comparative Biology*, 56, 449–458.
- Godoy, P.L. (2020) Crocodylomorph cranial shape evolution and its relationship with body size and ecology. *Journal of Evolutionary Biology*, 33, 4–21.
- Godoy, P.L., Montefeltro, F.C., Norell, M.A. and Langer, M.C. (2014) An additional baurusuchid from the cretaceous of Brazil with evidence of interspecific predation among crocodyliformes. *PLoS ONE*, 9, e97138.
- Godoy, P.L., Bronzati, M., Eltink, E., et al. (2016) Postcranial anatomy of *Pissarrachampsia sera* (Crocodyliformes, Baurusuchidae) from the Late Cretaceous of Brazil: insights on lifestyle and phylogenetic significance. *PeerJ*, 4, e2075.
- Godoy, P.L., Ferreira, G., Montefeltro, F.C., Vila Nova, B.C., Butler, R.J. and Langer, M.C. (2018) Evidence for heterochrony in the cranial evolution of fossil crocodyliforms. *Palaeontology*, 61, 543–558.
- Godoy, P.L., Benson, R.B.J., Bronzati, M. and Butler, R. (2019) The multi-peak adaptive landscape of crocodylomorph body size evolution. *BMC Evolutionary Biology*, 19, 167.
- Guillette, L.J. Jr., Edwards, T.M. and Moore, B.C. (2007) Alligators, contaminants and steroid hormones. *Environmental Sciences*, 14, 331–347.
- Holliday, C. and Witmer, L.W. (2009) The epipterygoid of crocodyliforms and its significance for the evolution of the orbitotemporal region of eusuchians. *Journal of Vertebrate Paleontology*, 29, 715–733.
- Holliday, C., Tsai, H., Skiljan, R., George, I. and Pathan, S. (2013) A 3D interactive model and atlas of the jaw musculature of *Alligator mississippiensis*. *PLoS ONE*, 8, e62806.
- Lautenschlager, S. (2015) Estimating cranial musculoskeletal constraints in theropod dinosaurs. *Royal Society Open Science*, 2, 150495.
- Lloyd, G.T., Davis, K.E., Pisani, D., et al. (2008) Dinosaurs and the Cretaceous terrestrial revolution. *Proceedings of the Royal Society B*, 275, 2483–2490.
- Mannion, P., Benson, R., Carrano, M., Tennant, J., Judd, J. and Butler, R. (2015) Climate constrains the evolutionary history and biodiversity of crocodylians. *Nature Communications*, 6, 8438.
- Marsola, J.C.A., Batezelli, A., Montefeltro, F.C., Grellet-Tinner, G. and Langer, M.C. (2016) Palaeoenvironmental characterization of a crocodylian nesting site from the Late Cretaceous of Brazil and the evolution of crocodyliform nesting strategies. *Palaeogeography, Palaeoclimatology, Palaeoecology*, 457, 221–232.
- Melstrom, K.M. and Irmis, R.B. (2019) Repeated evolution of herbivorous crocodyliforms during the Age of Dinosaurs. *Current Biology*, 29, 2389–2395.
- Montefeltro, F.C. (2019) The osteoderms of baurusuchid crocodyliforms (Mesoeucrocodylia, Notosuchia). *Journal of Vertebrate Paleontology*, 39, e1594242.
- Montefeltro, F.C., Larsson, H.C.E. and Langer, M.C. (2011) A new baurusuchid (Crocodyliformes, Mesoeucrocodylia) from the late cretaceous of Brazil and the phylogeny of Baurusuchidae. *PLoS ONE*, 6, e21916.
- Pol, D. and Leardi, J. (2015) Diversity patterns of Notosuchia (Crocodyliformes, Mesoeucrocodylia) during the Cretaceous of

- Gondwana. In: Fernández, M. and Herrera, Y. (Eds.) *Reptiles Extintos - Volumen en Homenaje a Zulma Gasparini*. Buenos Aires: Publicación Electrónica de la Asociación Paleontológica Argentina, pp. 172–186.
- Porro, L., Holliday, C., Anapol, F., Ontiveros, L., Ontiveros, L. and Ross, C. (2011) Free body analysis, beam mechanics, and finite element modeling of the mandible of *Alligator mississippiensis*. *Journal of Morphology*, 272, 910–937.
- Rayfield, E. (2004) Cranial mechanics and feeding in *Tyrannosaurus rex*. *Proceedings of the Royal Society B*, 271, 1451–1459.
- Rayfield, E. (2005) Aspects of comparative cranial mechanics in the theropod dinosaurs *Coelophysis*, *Allosaurus* and *Tyrannosaurus*. *Zoological Journal of the Linnean Society*, 144, 309–316.
- Rayfield, E. (2011) Structural performance of tetanuran theropod skulls, with emphasis on the Megalosauridae, Spinosauridae and Carcharodontosauridae. *Special Papers in Palaeontology*, 86, 241–253.
- Rayfield, E. and Milner, A. (2008) Establishing a framework for archosaur cranial mechanics. *Paleobiology*, 34, 494–515.
- Rayfield, E., Norman, D.B., Horner, C.C., et al. (2001) Cranial design and function in a large theropod dinosaur. *Nature*, 409, 1033–1037.
- Reed, D.A., Porro, L.B., Iriarte-Diaz, J., et al. (2011) The impact of bone and suture material properties on mandibular function in *Alligator mississippiensis*: testing theoretical phenotypes with finite element analysis. *Journal of Anatomy*, 218, 59–74.
- Riff, D. and Kellner, A. (2011) Baurusuchid crocodyliforms as theropod mimics: Clues from the skull and appendicular morphology of *Stratiotosuchus maxhechti* (Upper Cretaceous of Brazil). *Zoological Journal of the Linnean Society*, 163(suppl\_1), S37–S56.
- Sakamoto, M. (2010) Jaw biomechanics and the evolution of biting performance in theropod dinosaurs. *Proceedings of the Royal Society B*, 277, 3327–3333.
- Sakamoto, M., Ruta, M. and Venditti, C. (2019) Extreme and rapid bursts of functional adaptations shape bite force in amniotes. *Proceedings of the Royal Society B*, 286, 20181932.
- Sellers, K., Middleton, K., Davis, J. and Holliday, C. (2017) Ontogeny of bite force in a validated biomechanical model of the American alligator. *Journal of Experimental Biology*, 220, 2036–2046.
- Torices, A., Wilkinson, R., Arbour, V.M., Ruiz-Omenaca, J.I. and Currie, P.J. (2018) Puncture-and-pull biomechanics in the teeth of predatory coelurosaurian dinosaurs. *Current Biology*, 28, 1467–1474.
- Verdade, L.M. (2000) Regression equations between body and head measurements in the broad-snouted caiman (*Caiman latirostris*). *Revista Brasileira de Biologia*, 60, 469–482.
- Wilberg, E.W. (2017) Investigating patterns of crocodyliform cranial disparity through the Mesozoic and Cenozoic. *Zoological Journal of the Linnean Society*, 181, 189–208.
- Wilberg, E.W., Turner, A.H. and Brochu, C.A. (2019) Evolutionary structure and timing of major habitat shifts in Crocodylomorpha. *Scientific Reports*, 9, 1–10.
- Witmer, L. and Ridgely, R. (2008) The paranasal air sinuses of predatory and armored dinosaurs (Archosauria: Theropoda and ankylosauria) and their contribution to cephalic structure. *Anatomical Record*, 291, 1362–1388.
- Zanno, L. and Makovicky, P. (2013) Neovenatorid theropods are apex predators in the Late Cretaceous of North America. *Nature Communications*, 4, 2827.

**How to cite this article:** Montefeltro FC, Lautenschlager S, Godoy PL, Ferreira GS, Butler RJ. A unique predator in a unique ecosystem: modelling the apex predator within a Late Cretaceous crocodyliform-dominated fauna from Brazil. *J. Anat.* 2020;237:323–333. <https://doi.org/10.1111/joa.13192>